Mateo-Mateo, D.; Esteve-Adell, I.; Albero-Sancho, J.; Primo Arnau, AM.; García Gómez, H. (2017). Oriented 2.0.0 Cu2O nanoplatelets supported on few-layers graphene as efficient visible light photocatalyst for overall water splitting. Applied Catalysis B Environmental. 201:582-590. https://doi.org/10.1016/j.apcatb.2016.08.033

Oriented 2.0.0 Cu_2O nanoplatelets supported on few-layers graphene as efficient visible light photocatalyst for overall water splitting

Diego Mateo[a], Iván Esteve-Adell[a], Josep Albero[a], Ana Primo[a], Hermenegildo García[a,*]

[a] *Instituto de Tecnología Química, Universitat Politècnica de València-consejo Superior de Investigaciones Científicas, Avenida de los Naranjos s/n, 46022 Valencia, Spain*

Article history:

Received 26 May 20xx

Revised 9 June 20xx

Accepted 29 June 20xx

Available online

Abstract

Cu_2O nanoplatelets with preferential 2.0.0 facet orientation supported on few layers graphene were prepared as films in a single step by pyrolysis at 900 ºC under inert atmosphere of Cu^{2+}-chitosan precursor. $\overline{Cu_2O}$/fl-G films exhibit a photocatalytic activity for overall water splitting of 19.5 mmol/g_{Cu+G}·h. This value is about 4 orders of magnitude higher than the photocatalytic activity measured for unoriented Cu_2O nanoparticles on few-layers graphene or than commercial Cu_2O nanoparticles and about three orders of magnitude higher than the activity reported in the literature for Cu_2O nanoparticles. In addition Cu_2O nanoparticles on few-layers graphene retain about 50 % of its photocatalytic activity after 6 days of continuous irradiation. It is proposed that this activity and stability arises from the combination of features derived from the pyrolysis preparation procedure including strong Cu_2O–graphene grafting, the role of graphene as cocatalyst and preferential 2.0.0 facet orientation.

Key words: preferential orientation, photocatalysis, graphene, nanoplatelet, water splitting

*** Corresponding author.** Tel: +34 96 387 7807; Fax: +34 96 387 7809; E-mail: hgarcia@qim.upv.es

1. Introduction

Supported metal nanoparticles (MNPs) on high surface area solids have been extensively used in heterogeneous catalysis to promote a large variety of organic reactions [1, 2] including reductions [3], oxidations [4] and cross-couplings [5]. More recently, supported MNPs are finding increasing application for energy production and storage [6, 7].

There are ample precedents showing that the catalytic activity of supported MNPs can be strongly influenced by the support [8, 9]. In this regard, graphene (G), which constitutes the physical limit of 2D materials, is attracting much interest not only as metal-free catalyst, but also as support of MNPs [10-12]. The interest in the use of G as support derives from its unique properties, including large surface area, high adsorption capacity, possibility to form films coating arbitrary substrates and, importantly, the

strong MNP-G interaction that may arise from the overlap of the extended π orbital of G with the d orbitals of transition metals [12-15].

More relevant to our work, MNPs supported on G have been reported to exhibit photocatalytic activity [16, 17], including H_2 evolution from water containing sacrificial electron donors. Supported noble MNPs (Pt, Au, Ag etc.) have been widely reported in the literature as co-catalysts to increase the efficiency of photocatalytic H_2 generation under UV or/and visible light irradiation [18-20]. However, the use of critical metals can be a strong limitation for the wide applicability of these photocatalysts for H_2 generation and it is much more convenient the use of Earth-abundant and low-cost metals, such as Cu. In this regard, Cu_2O is a relatively non-toxic substance that exists abundantly in Nature as cuprite. Cu_2O is a semiconducting oxide with 2.0 eV band gap capable to promote photocatalytic water splitting upon visible light irradiation [21]. Domen and co-workers reported the photocatalytic overall decomposition of water into H_2 and O_2 on Cu_2O particles of 300-500 nm size upon irradiation with visible light in the absence of any sacrificial electron donor at rates of approximately 2 μmol/g·h without observing decrease in the H_2 evolution for more than 1900 h [22]. The photocatalytic activity of Cu_2O to promote the overall water splitting has been later confirmed other research groups [23-25] and supported by first-principles calculations that show that the conduction and valence bands of most stable facets of Cu_2O should have enough energy to promote overall water splitting and CO_2 reduction [26].

In the area of catalysis by MNPs, theoretical as well as scattered experimental data have shown that different crystallographic planes may exhibit different specific activity [27, 28]. Accordingly, there has been an increasing interest in controlling the preferential facets of MNPs exposed to the reaction to determine the influence of this parameter on the (photo)catalytic activity of MNPs. Specifically in the case of the photocatalytic overall water splitting into H_2 and O_2, Lee et al. found that the morphology of Cu_2O NPs influences their activity and stability for H_2 production from water upon visible light irradiation [24]. In that work, cubes, octahedra and rhombic dodecahedra, exhibiting, respectively, preferential (1.0.0), (1.1.1) and (1.1.0) facets, presented a H_2 production of 0, 0.5 and 1.6 μmol/g·h, for each type of crystallite. However, a fast degradation of the photocatalytic activity was found due to photocorrosion of Cu_2O to CuO during the H_2 production, resulting in unacceptable poor stability. The influence of the crystallographic facets of Cu_2O on the band energies and stability has also been addressed using DFT calculations [26]. Thus, it would be important to find a way to prepare oriented Cu_2O nanoparticles stable under photocatalytic H_2 generation.

In the present manuscript, we have prepared by a novel one-step pyrolysis procedure [29] oriented Cu_2O nanoplatelets having preferential (2.0.0) facet orientation strongly interacting with few–layers G ($\overline{Cu_2O}$/*fl*-G, $\overline{Cu_2O}$ meaning 2.0.0 oriented, *fl* meaning few layers) exhibit much higher photocatalytic activity for overall H_2O splitting in the absence of any sacrificial electron agent than those photocatalysts of Cu_2O previously reported or than analogous materials based on unoriented Cu_2O supported on fl-G (Cu_2O-fl-G). A remarkable positive influence of (2.0.0) facet orientation, strong metal oxide-support interaction and electron mobility on G on the photocatalytic activity has been established by comparing the H_2 evolution of oriented and unoriented Cu_2O NPs adsorbed on few layers G (Cu_2O/*fl*-G) under visible light irradiation (Scheme 1). As consequence of these favorable features the $\overline{Cu_2O}$/*fl*-G photocatalyst produced at least three magnitude orders higher H_2 production (in the range of mmol/g_{Cu}·h rather than μmol/g_{Cu}·h) respect the unoriented Cu_2O/*fl*-G film or suspended Cu_2O NPs. In addition, in spite of the small average particle size of oriented Cu_2O nanoplatelets compared to those in the micrometric length scale reported in the literature, [22] it was found that these $\overline{Cu_2O}$/*fl*-G samples can operate for six days without appreciable change in the morphology and retaining a considerable percentage of its photocatalytic activity, thus proving the remarkable stability under photocatalytic

conditions.

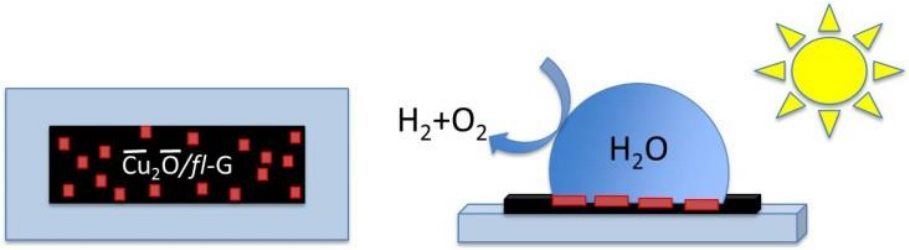

Scheme 1. Pictorial representation of a frontal view of films of oriented Cu_2O nanoplatelets (small orange squares) supported on few-layers G (black large rectangle) deposited on a quartz substrate (light blue rectangle) and the process of photocatalytic H_2 and O_2 evolution from pure, liquid H_2O without stirring using the $\overline{Cu_2O}$/*fl*-G film on quartz (presented in a lateral view) illuminated with UV-Vis light.

2. Experimental

2.1. Synthesis of catalyst

Preparation of $\overline{Cu_2O}$/*fl*-G. $\overline{Cu_2O}$/*fl*-G films were prepared as reported before [29]. In brief, chitosan (0.5 g) from Aldrich (low molecular weight) was dissolved in a copper (II) nitrate aqueous solution (18 mg of $Cu(NO_3)_2 \cdot 2\ H_2O$ in 25 ml of water) by addition of 0.23 g of acetic acid. To remove insoluble impurities typically present in commercial chitosan, the he solution was filtered through a syringe having a membrane filter of 0.45 µm diameter pore size. Films of chitosan containing $Cu(NO_3)_2$ coating quartz plates (2 × 2 cm^2) were obtained by casting 300 µl of filtered solution at 6,000 r.p.m. in 1 min. Conversion of chitosan into graphene and formation of Cu metal nanoparticles was performed by pyrolysis under argon atmosphere in a tubular oven heating at a rate of 5 $^0C \cdot min^{-1}$ up to 900 ^0C with a hold time of 2 h. The sample was, then, cooled at room temperature under argon. The resulting sample immediately after the pyrolysis consisted in metallic Cu nanoplatelets grafted on G that undergo spontaneous Cu oxidation to $\overline{Cu_2O}$/*fl*-G. upon exposure to the ambient. The samples used in the present study were aged for at least two days, before being used as photocatalysts.

Preparation of Cu_2O/fl-G.

A suspension of few-layers graphene in ethylene glycol (40 ml) was obtained by sonication at 700 W for 1 h a carbon residue (100 mg) obtained from the pyrolysis of alginic acid sodium salt from brown algae (Aldrich) until a well dispersed fl-G ink was observed. $CuCl_2$ (1.06 mg for the preparation of the sample at 0.1 wt% Cu_2O) was added to the reaction mixture and Cu metal reduction was then performed at 120 ^0C for 24 h under continuous stirring. The Cu/fl-G were finally recovered by filtration and washed exhaustively with water and with acetone. The resulting material was dried in a vacuum desiccator at 110 ^oC to remove the remaining water. Spontaneous oxidation of Cu/fl-G by exposure to the ambient for longer than two days renders the control sample Cu_2O/fl-G having unoriented Cu_2O NPs. Preparation of films of unoriented Cu_2O on quartz for XRD measurements was performed by casting a few drops of a suspension of Cu_2O/fl-G on water freshly prepared by ultrasonication on a clean quartz slide.

Ethanolic suspension of Cu_2O was purchased from Aldrich (1.5% (w/v)).

The amount of copper present in the samples was determined by inductively coupled plasma-optical emission spectrometry (ICP-OES) by immersing the plates into aqua regia at room temperature for 3 h and analyzing the Cu content of the resulting solution.

2.2. Characterization of catalyst

Powder XRD patterns were recorded on a Shimadzu XRD-7000 diffractometer using Cu *Kα* radiation (λ = 1.5418 Å, 40 kV, 40 mA) at a scanning speed of 1 ^{0} per min in the 10-80^0 2Θ range.

Raman spectrum was collected with a Horiba Jobin Yvon-Labram HR UV-Visible-NIR (200-1,600 nm) Raman Microscope Spectrometer, using a laser with the wavelength of 632 nm. The spectrum was collected from 10 scans at a resolution of 2 cm^{-1}.

Scanning electron microscopy (SEM) images were recorded with a Zeiss Ultra 55 field emission scanning electron microscope (FESEM) apparatus. The crystal phase of the Cu NPs was determined by FESEM using an electron backscatter diffraction detector inside the chamber and transmission electron microscopy (TEM) after removal of the quartz substrate. Besides XRD, direct evidence of preferential morphology and facet orientation of Cu_2O particles in $\overline{Cu_2O}$/*fl*-G films was also determined by TEM. In the case of $\overline{Cu_2O}$/*fl*-G films on quartz, TEM imaging required the prior detachment of $\overline{Cu_2O}$/*fl*-G from the quartz substrate with the minimal alteration of the orientation of the particles. This was performed by consecutive careful mechanical polishing of quartz up to 100 nm thickness, followed dimpling grinding and final argon ion milling until complete removal of quartz. The resulting self-standing $\overline{Cu_2O}$/*fl*-G film detached from quartz was introduced directly in the TEM chamber without deposition on a holey copper grid. Preferential facet orientation of Cu_2O nanoplatelets was deduced from comparison of the TEM image with that of the image presenting only those Cu_2O nanoplatelets exhibiting the electron diffraction pattern corresponding to (2.0.0) orientation.

XPS spectra were measured on a SPECS spectrometer equipped with a Phoibos 150 9MCD detector using a non-monochromatic X-ray source (Al and Mg) operating at 200 W. The samples were evacuated in the prechamber of the spectrometer at $1 \cdot 10^{-9}$ mbar. The measured intensity ratios of the components were obtained from the area of the corresponding peaks after nonlinear Shirley-type background subtraction and corrected by the transition function of the spectrometer.

Atomic force microscopy (AFM) measurements were conducted in the contact mode in air at ambient temperature using a Veeco AFM apparatus. It should be noted that AFM were not measured in a clean room and, therefore, films on quartz substrates may contain dust that will be detectable by these techniques.

Transient absorption (TAS) experiments were recorded using a home-built system as reported before [30]. The samples were excited with a Nd:YAD laser at 532 nm and 1 Hz.

2.3. Photocatalytic measurements

The $\overline{Cu_2O}$/*fl*-G films supported on quartz or any other photocatalyst were introduced in a sealed orthogonal photoreactor (20×10×4 cm^3) of aluminum body and a top quartz window. Ar-purged water was spread on top of the $\overline{Cu_2O}$/*fl*-G film until complete film coverage. The H_2 evolution tests were determined by connecting directly the photoreactor to an Agilent 490 Micro GC (Molsieve 5A column with Ar as carrier gas). The light source was a 300 W Xe lamp. The lamp was located at 13 cm distance from the films, achieving an irradiance of 160 $mW \cdot cm^{-2}$ on the films surface. The temperature and pressure inside the reactor was controlled through a thermocouple and a manometer, respectively. The temperature of the system never overcomes 50 ^{o}C, apart from the case of the temperature-production dependence experiments. The photocatalytic activity of each sample was evaluated at least in three independent experiments, without observing significant differences among the various tests.

3. Results and discussion

3.1. Photocatalyst characterization

Oriented $\overline{Cu_2O}$/*fl*-G films were prepared as reported by pyrolysis at 900 ºC under inert atmosphere of a Cu^{2+}-chitosan film of nanometric thickness on quartz and spontaneous oxidation by exposure to the ambient atmosphere, except that for the present application high Cu loading was found beneficial. [33] The process forms initially metallic Cu particles that are subsequently converted into Cu_2O. Characterization by ICP-OES elemental analysis showed that the Cu content of the most efficient $\overline{Cu_2O}$/*fl*-G films prepared was 4.75 µg/cm^2. As it can be observed in the FESEM images of **Figure 1**, Cu_2O nanoplatelets appeared homogeneously distributed on the few-layers G support. From these images at different magnifications a bimodal size distribution was observed. The average size of each type of nanoplatelet was determined by measuring a statistically relevant number of particles. The smallest ones exhibit a size distribution between 5 and 20 nm with an average about 8 nm. The biggest nanoplatelets have a broader distribution between 40 and 200 nm and an average of 130 nm. Moreover, AFM images confirm the uniform nanoplatelet distribution over the few-layers G sheet (20 nm thickness) and the presence of two main size groups with a uniform height of about 20-30 nm (see **Figure S1** in Supplementary Information). The origin of this bimodal distribution is probably related to the preparation procedure of $\overline{Cu_2O}$/*fl*-G films and the mechanism in which Cu nanoplatelets are generated and grow during the pyrolysis at 900 ºC by agglomeration of small melted Cu nanodrops on G. Thus, large Cu_2O nanoplatelets are surrounded by a circular zone in where small Cu_2O particles are located having a central larger particle.

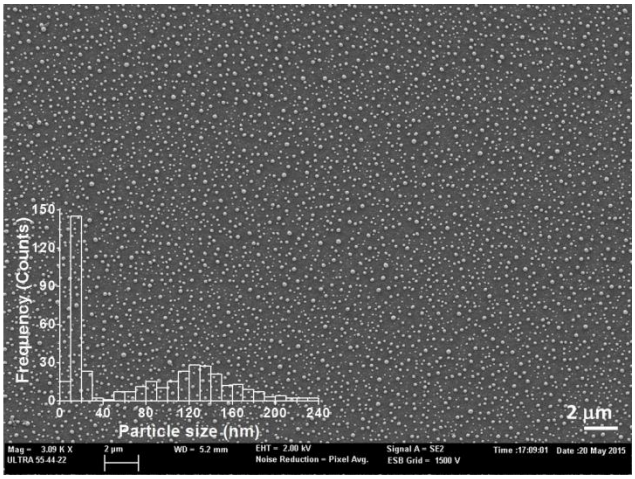

Figure 1. Large field FESEM image of an efficient $\overline{Cu_2O}$/*fl*-G film two days after preparation showing the homogeneous distribution of $\overline{Cu_2O}$ nanoplatelets on *fl*-G. The nanoplatelet size distribution histogram is presented as inset and shows a bimodal distribution with more abundant small size nanoplatelets. At the magnification presented only large particles can be observed.

Raman spectroscopy of $\overline{Cu_2O}$/*fl*-G films showed the corresponding D and G bands expected for graphene sheets with defects due to the presence of residual oxygenated functional groups remaining from the initial polysaccharide precursor (see insert in **Figure 2**). In addition, the low frequency region of the Raman spectra shows the characteristic vibration bands of Cu_2O at 635, 436 and 218 cm^{-1}, providing information of the oxidation state of the Cu species (a magnified image of this region can be seen in **Figure S2** in supplementary Information). While metallic Cu(0) is silent in Raman spectroscopy and it does not exhibit any specific absorption peak, CuO exhibits characteristic vibration

bands at 615, 330 and 280 cm^{-1} that in the present case of $\overline{Cu_2O}$/*fl*-G films were below the detection limit [31, 32]. This agrees with previous observations that G stabilizes preferentially Cu(I) oxidation state over Cu(II) that are formed by spontaneous oxidation of metallic Cu particles [33, 34].

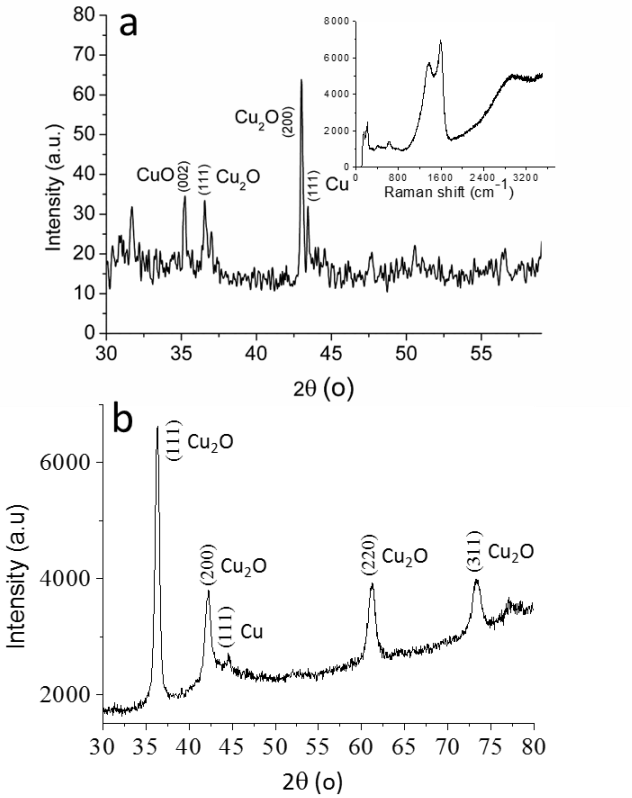

Figure 2. a) XRD pattern recorded for the $\overline{Cu_2O}$/*fl*-G film (4.75 µg/cm^2) two days after its preparation in which the corresponding peaks have been indexed. The inset shows the corresponding Raman spectrum of the sample recorded with 512 nm excitation. Note that the peaks appearing in the Raman spectrum at wavenumbers below 800 cm^{-1} are attributable to Cu_2O; b) XRD of unoriented Cu_2O/fl-G film that agrees well with reported patterns for conventional Cu_2O smples. Note that the area of the (1.1.1) peak is 2.5 fold higher than that of (2.0.0) for unoriented Cu_2O/fl-G, while in the case of $\overline{Cu_2O}$/*fl*-G film the (2.0.0) peak is about 3 times larger than that corresponding to the (1.1.1) facet.

In the related precedent, the low concentration of Cu present on fl-G (2.5 ng/cm^2) precluded the observation of any XRD pattern characteristic of Cu species. In the present case, the much higher Cu_2O loading has allowed us recording a XRD of $\overline{Cu_2O}$/*fl*-G films (4.75 µg/cm^2). **Figure 2** presents the XRD pattern of a $\overline{Cu_2O}$/*fl*-G film two days after its preparation. For the sake of comparison **Figure 2** also presents the XRD of an unoriented Cu_2O/fl-G film, whose XRD agrees well with the conventional XRD pattern expected for Cu_2O. Unoriented Cu_2O NPs were synthesized by ambient oxidation of Cu NPs obtained from the polyol method and supported on fl-G (see experimental section). On one hand, XRD of the $\overline{Cu_2O}$/*fl*-G film confirms the presence of Cu_2O as predominant species over metallic Cu or CuO. On the other hand, XRD also proves the preferential (2.0.0) facet orientation of Cu_2O nanoplatelets based on the relative higher intensity of the corresponding peak over the (1.1.1) and the rest of XRD peaks.

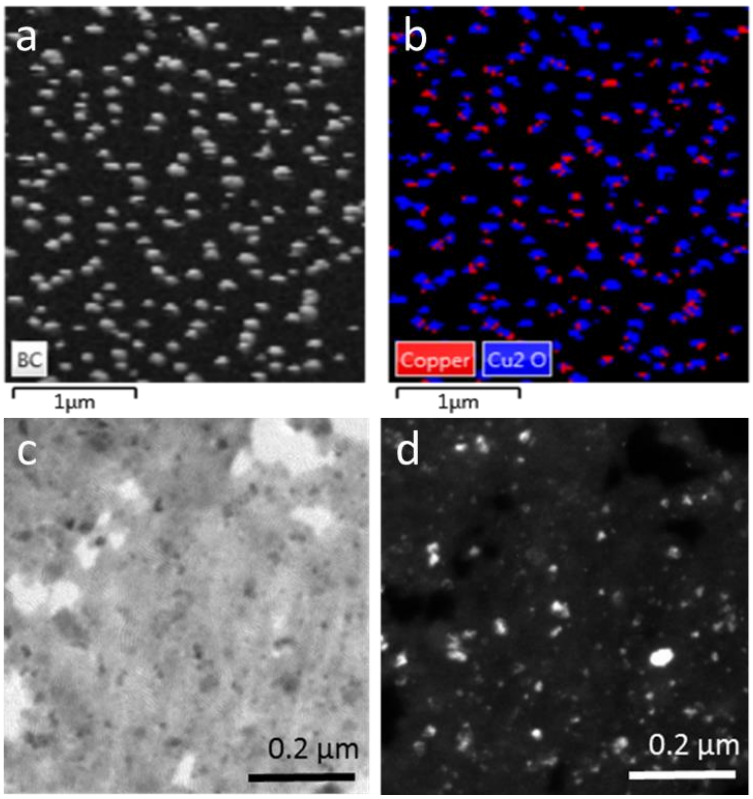

Figure 3. a: FESEM image of $\overline{Cu_2O}$/*fl*-G film two days after preparation. b: Image of the same area as a, but obtained by overlapping the particles having the electron diffraction corresponding to Cu(I) (blue) and Cu(0) (red). c: TEM image of self-supported $\overline{Cu_2O}$/*fl*-G film after removal of quartz substrate. The holes of the film are due to the process of mechanical removal of quartz. d: Image of the same area as c, but presenting only those Cu_2O particles that have the characteristic electron diffraction of the 2.0.0 facet.

Besides XRD, prevalence of Cu_2O over other oxidation states of Cu and preferential orientation of Cu_2O nanoplatelets in $\overline{Cu_2O}$/*fl*-G films was also confirmed by electron microscopy. **Figure 3** a and b shows a comparison of the FESEM image with that provided by electron backscattering diffraction of the same region. The coincidence between the two images indicates that most of the nanoplatelets in this $\overline{Cu_2O}$/*fl*-G film correspond to Cu_2O. Preferential 2.0.0 facet orientation of Cu_2O nanoplatelets was assessed by TEM imaging after removing the quartz substrate from the $\overline{Cu_2O}$/*fl*-G film by a combination of mechanical polishing, dimpling grinding and Ar ion sputtering to avoid alteration of the orientation of Cu_2O nanoplatelets. The self-standing $\overline{Cu_2O}$/*fl*-G films could be observed by transmission techniques. Comparison of the TEM image with that corresponding to the fraction of those particles showing 2.0.0 facet orientation is provided in **Figure 3** panels c and d. Using ImageJ software, it was estimated that about 85% of the Cu_2O nanoplatelets observed in TEM have 2.0.0 facet orientation.

Figure 4 shows the high resolution XPS spectra, C1s and Cu2p peaks and the best deconvolution to individual components. As it can be seen in this Figure, XP spectra show the presence of Cu(I) (933 eV peak) and Cu(II) (935 eV peak) on the outermost layers of the oriented $\overline{Cu_2O}$/*fl*-G film. Since Cu(II) was not detected neither in Raman spectroscopy nor in FESEM imaging, it can be concluded the presence of this oxidation state has to be limited just to a shallow outermost layer of Cu_2O nanoplatelets of less than a few nm. In addition, Auger peak reveals that the absence of Cu(0) on the external layers of the nanoplatelets (see **Figure S3**). C1s peak in XPS showed narrow 284.5 eV peak corresponding to

graphenic C-C and two minor components (< 5 atom %) attributable to C atoms bonded to an O and/or a N atoms. The presence of N atoms on the graphene resulting from the pyrolysis of chitosan has been previously reported [35]. Surprisingly, although in previous reports the presence of N atoms in $\overline{Cu_2O}$/*fl*-G films was not observed in the present case N atoms (about 0.8 %) have been detected. Overall all the available characterization data are in agreement with those recently reported for $\overline{Cu_2O}$/*fl*-G films obtained using the same procedure, indicating the predominant presence of (2.0.0) oriented Cu_2O nanoplatelets strongly grafted on few layers graphene [29].

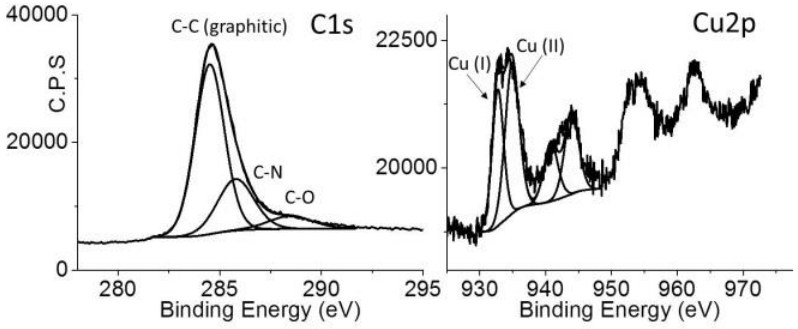

Figure 4. XPS recorded for a $\overline{Cu_2O}$/*fl*-G film (4.75 μg Cu cm^{-2}) showing the experimental C1s (a) and the Cu2p (b) peaks and their best deconvolution to individual components, as indicated in the panels.

3.2. Photocatalytic measurements

The purpose of the present study was to test the photocatalytic activity of $\overline{Cu_2O}$/*fl*-G films on quartz for overall water splitting. Towards this goal, a film of $\overline{Cu_2O}$/*fl*-G (5.8 μg (Cu+G) / cm^2) was placed in a closed reactor under Ar atmosphere and previously Ar-purged water drops were put on the film. The $\overline{Cu_2O}$/*fl*-G film wetted with the water drops on top of it was irradiated at ambient temperature without any stirring with UV-Vis light with a 300 W Xe lamp (160 mW/cm^2) at 13 cm distance (see **Scheme 1**). It is worth to note that after 24 h irradiation some liquid water was still visually remaining on top of the films. The temperature of the $\overline{Cu_2O}$/*fl*-G film never overcomes 50 ºC in most of the experiments. However, to determine the influence of the temperature on the photocatalytic overall water splitting an additional experiment was carried out at 75 ºC, by heating the stainless steel photoreactor with a hot plate and controlling the internal temperature with a thermocouple. At this temperature, a decrease in the H_2 production rate of approximately 50 % was observed (9.2 $mmol/g_{Cu+G}\cdot h$) compared with non-heated photocatalytic experiments. This behavior is not surprising since recombination rates in semiconductors usually increase with temperature, and therefore the yield of hydrogen production should be diminished when temperature increases due to a more efficient electron/hole recombination. It is also important to indicate that mechanocatalytic H_2 generation previously reported for Cu_2O cannot contribute in the present case to any H_2 generation due to the static conditions and the absence of any type of stirring [36, 37]. No gas evolution was observed in the dark with the lamp on but covering the photoreactor with aluminium foil. In contrast, generation of H_2 and O_2 was observed in all the experiments upon illumination of $\overline{Cu_2O}$/*fl*-G in the absence of any sacrificial electron donor. The temporal evolution of the photocatalytic H_2 and O_2 production is shown in **Figure 5**. A productivity value of 19.5 $mmol/g_{Cu+G}\cdot h$ and a turnover number of 68 mol H_2/mol Cu was reached at 24 h.

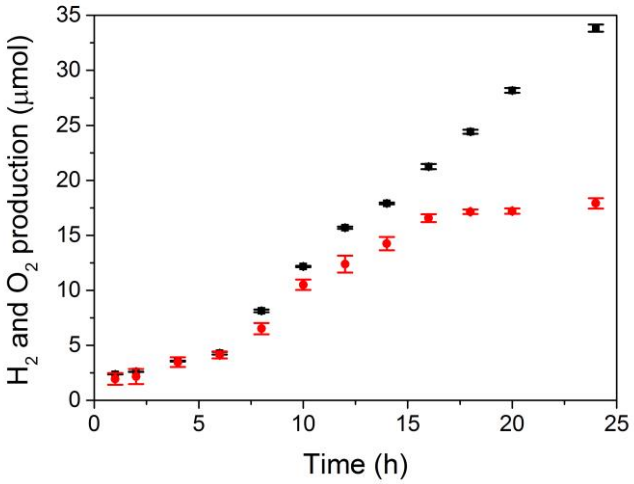

Figure 5. Raw H_2 (black squares) and O_2 (red dots) production from $\overline{Cu_2O}$/*fl*-G film (12.5 cm^2) as function of time upon UV-Vis light irradiation from a 300 W Xe lamp. The productivity data correspond to 19.5 mmol/g_{Cu+G} ·h.

For comparison, an aqueous dispersion of Cu_2O NPs without any preferential orientation supported in *fl*-G powder (Cu_2O/fl-G) was submitted to identical light irradiation. Unoriented Cu_2O NPs (7 nm average particle size) were synthetized by ambient oxidation of Cu NPs obtained from the polyol method and supported on fl-G (see experimental section). In addition, commercial Cu_2O NPs stabilized in ethanol (<350 nm particle size) were also used to test their photocatalytic H_2 evolution from water under UV-Vis light. In all cases, the simultaneous generation of H_2 and O_2 was observed, as reported in the literature for Cu_2O NPs [22]. The results of H_2 production using different photocatalysts and conditions are summarized in **Table 1** in where the average of three or more independent measurements and the corresponding estimated errors have been indicated.

Control experiments were carried out in the absence of light for which no H_2 evolution was detected. The use of oriented $\overline{Cu_2O}$/*fl*-G produced 4 orders of magnitude more H_2 than an active sample of unoriented Cu_2O NPs supported on fl-G (Cu+G content 30 mg, H_2 production 0.0046 mmol H_2/g_{Cu+G}·h). Note that if unoriented Cu_2O/fl-G having similar Cu content as $\overline{Cu_2O}$/*fl*-G (0.022 mg Cu, see **Table 1**) is irradiated, no H_2 evolution is observed under the same conditions, probably due to the very low photocatalytic activity of this sample of unoriented Cu_2O/fl-G film with a minute Cu_2O amount. This contrasting activity is indicating that the $\overline{Cu_2O}$/fl-G samples prepared by pyrolysis, exhibiting a strong $\overline{Cu_2O}$-G grafting and having preferential (2.0.0) orientation in the $\overline{Cu_2O}$/fl-G, are catalytically more active in the photocatalytic H_2 evolution than samples prepared by adsorption on preformed G that do not exhibit any preferential orientation. Moreover, in a related precedent, a superior H_2 production was demonstrated when rhombic dodecahedra Cu_2O NPs with (110) facets were used instead of Cu_2O cubes with (100) facets or octahedral with (111) facets [24], indicating that some specific orientations might present improved photocatalytic activity than others. Unfortunately, the synthetic procedure employed in this manuscript does not allow us controlling selectively at will the growth of different facets of Cu_2O on G and, therefore, it still remains to be determine if other facets could exhibit an even higher photocatalytic activity for H_2 evolution. However, what our results establish that the pyrolytic preparation procedure leading to the preferential orientation of one of the Cu_2O facets renders a material that is several orders of magnitude more efficient for the photocatalytic overall water splitting compared with unoriented samples.

It is very likely that the strong $\overline{Cu_2O}$-G interaction favors the interfacial electron transfer between the components of the photocatalytic system, rendering charge separation more efficient. This electron migration from a semiconductor to G is widely accepted as the reason why G as additive in a few weight percents increases the photocatalytic activity of TiO_2 and other semiconductors [25, 38]. In the present case, the one-step pyrolysis procedure for preparation of $\overline{Cu_2O}$/*fl*-G should be not only responsible for preferential 2.0.0 facet orientation of resulting Cu_2O, but also for strong grafting of $\overline{Cu_2O}$ nanoplatelets on fl-G.

In addition, control experiments confirmed that the use of commercial Cu_2O NPs in sufficient amount (2.665 mg) without graphene results in a weak photocatalytic activity, while *fl*-G without Cu_2O NPs did not show any catalytic activity. This is indicating that the only catalytically active site is the Cu_2O NPs, and G is acting firstly as support of the NPs, secondly as co-catalyst and also as templating agent favoring the preferential (200) facets orientation. It is worth noticing that commercial Cu_2O NPs has presented higher activity than unoriented Cu_2O/*fl*-G, but still orders of magnitude lower than that of $\overline{Cu_2O}$/*fl*-G. It should be commented that the possibility that some residual ethanol, favoring H_2 evolution in commercial Cu_2O NPs by acting as sacrificial electron donor cannot be totally excluded in this case since the commercial Cu_2O nanoparticles are stabilized in ethanol to avoid their oxidation.

It should be also commented that when similar amount of Cu_2O (50 μg Cu, see **Table 1**) as that present in $\overline{Cu_2O}$/*fl*-G films was used as photocatalyst for comparison, no evidence of photocatalytic H_2 generation was obtained and, for this reason, it was necessary to use higher amounts (2.665 mg) to observe H_2 evolution.

Table 1. H_2 production from water in the absence of sacrificial electron donors using oriented (entries 1-3) and non-oriented Cu_2O NPs (4 and 5) supported on few-layers G and Cu_2O NPs (entries 6 and 7) upon UV-Vis light irradiation from a 300 W Xe lamp

Photocatalyst	Cu+G amount (mg)[a]	Reaction time (h)	Average H_2 production (mmol/g·h)[b]
$\overline{Cu_2O}$/*fl*-G	0.072	24	19.5±0.3
$\overline{Cu_2O}$/*fl*-G [c]	0.099	24	3.70±0.01
Cu_2O/*fl*-G	30	17	0.0046±0.0001
Cu_2O/*fl*-G	0.022	20	-[d]
Cu_2O NPs	2.665	20	0.047±0.007
Cu_2O NPs	0.050	20	-[d]
Cu_2O NPs (0.3- 0.5 μm)	500	1900	0.004[e]
Ru_2O decorated	500	400	0.0008[f]

Cu_2O NPs			
Cu_2O NPs (100-300nm)	20	120	0.0013[g]

[a] For the hydrogen production the films total amounts has taken into account since G could have photocatalytic activity [b] Formation of O_2 in quasi stoichiometric amounts was observed; [c] Irradiated only with visible light using a cut-off filter of 405 nm; [d] No H_2 was detected.[e] Data reported in ref.[22], the photocatalytic experiment was carried out in a 200 cm^3 pyrex cell under a 300 W Xe lamp ($\lambda > 460$ nm). [f] Data obtained from ref. [39], the photocatalytic reaction was performed irradiating a pyrex cell with a 300 W Xe lamp ($\lambda >$ 450 nm).[g] Data obtained from ref. [40], the photocatalysis was carried out in a 20 cm^3 glass vessel with a 150 W halogen lamp (irradiation 350 mW/cm^2).

The extraordinary efficiency of $\overline{Cu_2O}$/*fl*-G film as photocatalyst compared to its congeners has to derive in part from the activity of fl-G as co-catalyst. To obtain some evidence of the photochemical generation of the state of charge separation upon irradiation of the $\overline{Cu_2O}$/*fl*-G film, transient absorption measurements of the film were performed using a pulsed ns laser system. Thus, monitoring at 600 nm a transient signal could be observed for the $\overline{Cu_2O}$/*fl*-G films upon 532 nm excitation under nitrogen. The intensity of the transient signal immediately after the laser pulse increased under air atmosphere. When excitation was carried out in the presence of methanol as electron donor disappearance of the transient signal was observed. **Figure 6 (a)** shows the temporal profiles of the transient signal monitored at 600 nm recorded for $\overline{Cu_2O}$/*fl*-G film under the various conditions. These results can be interpreted considering that the 600 nm signal is mostly due to positive holes reaching the microsecond timescale generated on Cu_2O upon photoexcitation, formation of the charge separation state and subsequent electron migration to fl-G. If this is the case, then the presence of O_2 should increase its initial intensity in the microsecond time scale as consequence of the lesser extent of prompt charge recombination of the hole with electrons, due to their trapping by O_2. In contrast, the presence of CH_3OH, a known electron donor, will make the signal of positive holes disappear completely. The lifetimes of these holes in $\overline{Cu_2O}$/*fl*-G film under N_2 and O_2 were estimated from the fitting of the signal to a first-order kinetics as τ_{N2} = 12.5 μs and τ_{O2} = 11.3 μs, respectively. Moreover, a control experiment submitting a suspension of commercial Cu_2O NPs in acetonitrile under air to laser excitation in the same conditions did not allow detecting any transient signal, indicating that G is effectively enhancing the lifetime of charge separation in $\overline{Cu_2O}$/*fl*-G films.

In view of the previous data, we could establish that the oxygen evolution reaction would take place fundamentally in the Cu_2O nanoplatelets after light excitation. Moreover, as it has been previously reported the Cu_2O valence band position would be enough oxidant to perform H_2O oxidation as can be observed in **Figure 6 (b)** [41]. Considering that the valence band energy of G has been reported as 5.94 V relative to the vacuum,[42] the most likely mechanism to explain the remarkable photocatalytic activity of is illustrated in Scheme 2.

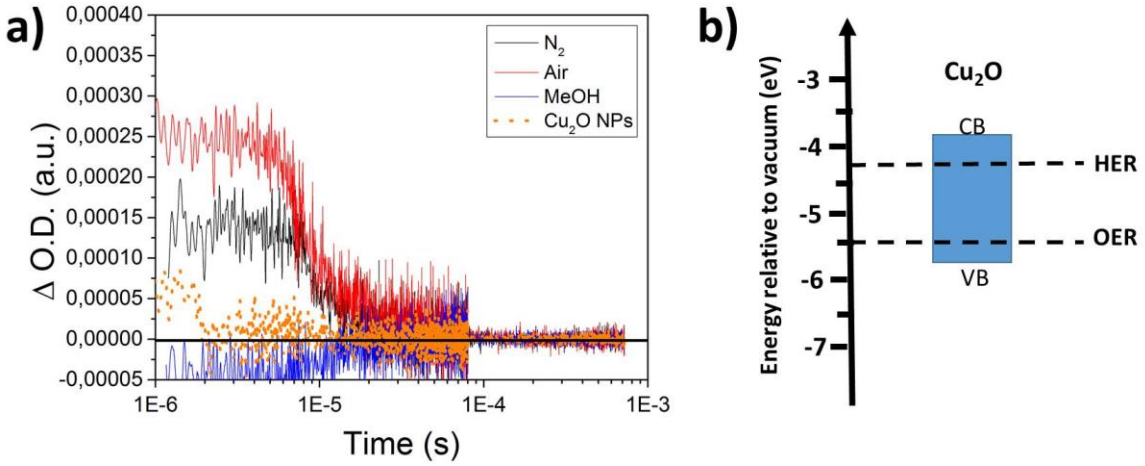

Figure 6. (a)Transient absorption kinetics of a $\overline{Cu_2O}$/*fl*-G film measured under N_2 (black), air (red) and MeOH (blue) atmospheres and Cu_2O NPs suspension (orange). The excitation wavelength was 532 nm, and the monitoring wavelength 600 nm. (b) Energy band alignment of Cu_2O respect oxygen and hydrogen evolution reactions.

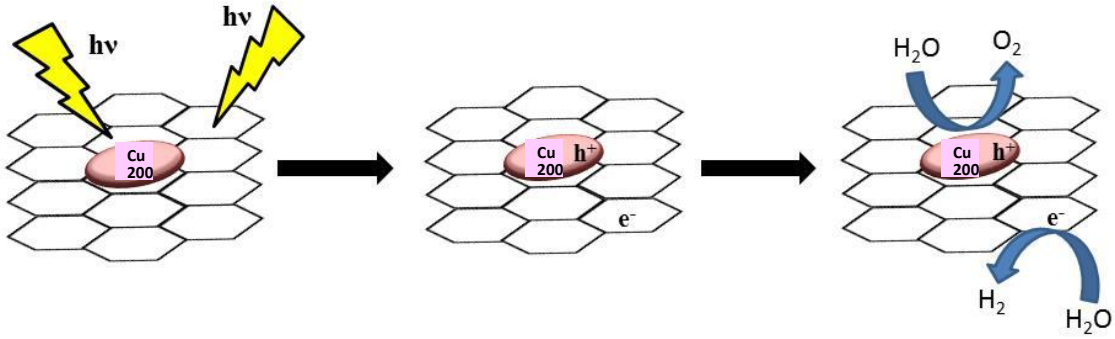

Scheme 2. Illustration of the role of *fl*-G enhancing the efficiency of charge separation and the overall photocatalytic efficiency of $\overline{Cu_2O}$/*fl*-G.

For $\overline{Cu_2O}$/*fl*-G, the H_2 and O_2 production was also measured under visible light using a cut-off filter of 405 nm. The H_2 evolution under visible light was 3.70 ± 0.01 mmol/g_{Cu+G}·h, as included in **Table 1**. This value is about 19% of the one obtained with full UV-Vis light irradiation, after correcting for the different amount of Cu_2O. This percentage indicates that the $\overline{Cu_2O}$/*fl*-G films are also notably active in the visible part of the spectrum. This is in accordance with the 2.0 eV bandgap of Cu_2O. [21] However, when using the unfiltered light from the Xe lamp, the UV region still contributes in a large extent to the overall activity than visible light.

The Cu amount in the reaction was increased by introducing in the reactor $\overline{Cu_2O}$/*fl*-G films (7.88 $\mu g_{Cu+G}/cm^2$) with larger surface (4,8 and 16 cm^2) in order to elucidate how the photocatalytic overall water splitting was affected by increasing the irradiation area and amount of oriented Cu_2O nanoplatelets. The photocatalytic H_2 evolution increased linearly with the Cu amount present in the photoreactor as it is presented in **Figure S4** in the supplementary information. In spite of the small amount of Cu in the G films (in the sub milligram scale), as soon as the Cu mass was increased, the H_2 and O_2 production increases as well.

3.2. Photocatalyst stability

Besides the improved H_2 and O_2 production due to the preferential orientation of the $\overline{Cu_2O}$ nanoplatelets, the use of fl-G as support produced also an enhanced stability when compared with non-supported Cu_2O NPs, which are well-known to rapidly oxidize to CuO under photocatalytic conditions [24]. In this regard, a $\overline{Cu_2O}$/*fl*-G film was placed in a crucible filled of Ar-purged water, and the reaction was followed for six days (**Figure 7**). As can be observed the photocatalyst still retains approximately about 50% of the activity even after 6 days under continuous irradiation. FESEM images of a six days used $\overline{Cu_2O}$/*fl*-G film showed no alterations in the particle size distribution, remaining the bimodal distribution as that shown in the inset of Figure 8, excluding any particle growth as the origin of the deactivation. However, nanoplatelets morphology was affected after six days reaction and as can be observed in **Figure 8a** the Cu_2O particles present a rough surface with an irregular shape. In order to investigate the origin of the changes in Cu_2O morphology, C1s and Cu2p XPS spectra of a $\overline{Cu_2O}$/*fl*-G film after 6 days reaction were recorded (**Figure 8b**). Although the C1s XPS spectrum did not present notable differences, the relative intensities of Cu(I) (933 eV) and Cu(II) (935 eV) peaks varied from the initial spectra presented in **Figure 4**. In this case, after six days reaction, the relative intensity of Cu(I) peak decreased respect the Cu(II) peak, indicating that a percentage of Cu(I) has evolved to Cu(II) during the six days reaction time. Thus, the most likely cause of deactivation is the partial transformation of Cu_2O into CuO, as it has been reported in the literature for unsupported particles.[24, 43] In any case, **Figure 7** indicates a considerable increase in the stability of the Cu_2O supported on *fl-G* under reaction conditions respect the non-supported Cu_2O NPs and previous investigations [24, 43].

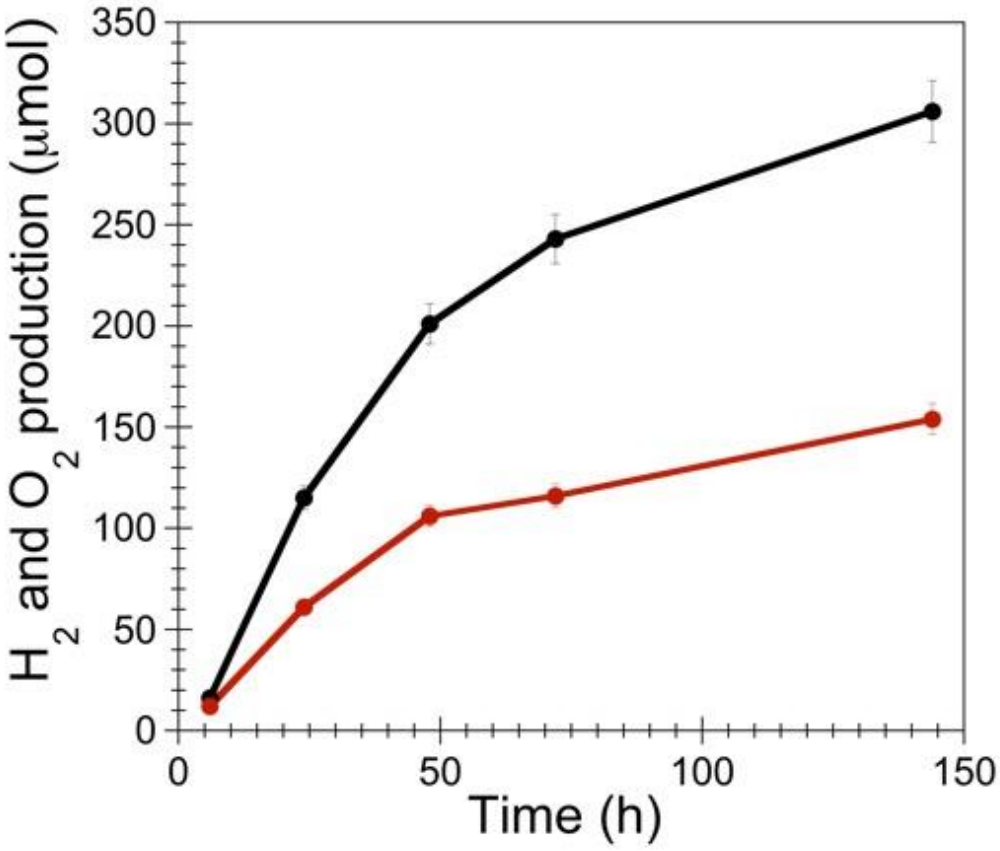

Figure 7. H_2 and O_2 production from a $\overline{Cu_2O}$/*fl*-G film containing 0.099 mg of Cu+G upon UV-Vis light irradiation from 300 W Xe lamp for six days.

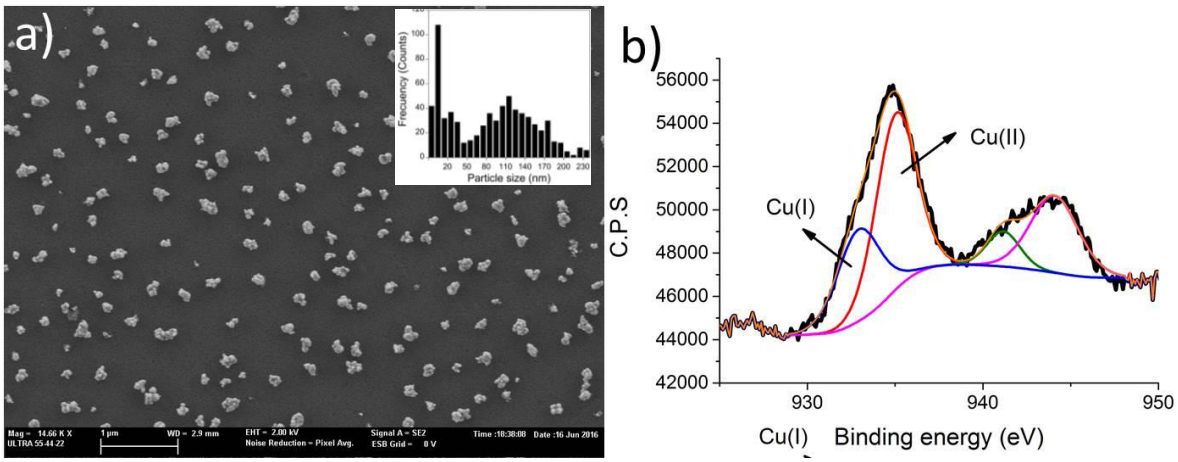

Figure 8. a) FESEM image from a $\overline{Cu_2O}$/*fl*-G film (4.75 μg Cu cm^{-2}) after six days reaction upon UV-Vis light irradiation from 300 W Xe lamp. The inset presents the particle size distribution histogram showing the bimodal distribution. b) Cu2p XPS spectrum of the same film. Note that no direct quantitative comparison with the Cu2p peak of Figure 4 can be made due to different acquisition times.

4. Conclusions

The use of preferentially oriented $\overline{Cu_2O}$ nanoplatelets strongly grafted on few layer G has demonstrated not only three to four orders of magnitude improved H_2 evolution for the overall water splitting compared the randomly oriented NPs, but also higher stability, exhibiting long-term H_2 production. This enhanced activity and stability appears to be due to the facet orientation, the strong $\overline{Cu_2O}$-graphene interaction and the role of G as cocatalyst. Thus, after photon absorption at Cu_2O and occurrence of charge separation, electrons migrate rapidly from Cu_2O to graphene, enhancing in this way the efficiency of charge separation. At this moment, holes should be located at Cu_2O and electrons on graphene. Further studies are directed to show that facet orientation of metal NPs on graphene is a general methodology to render an advanced generation of more efficient photocatalysts for solar fuel production.

Acknowledgments

Finantial support by the Spanish Ministry of Economy and Competitiveness (Severo Ochoa and CTQ2015-69153-CO2-1-R) and Generalitat Valenciana (Prometeo 2013-019) is gratefully acknowledged. D. M. M. and I. E. A thank to the Technical University of Valencia and the Spanish Ministry of Science for PhD scholarships.

References:

[1] J.M. Campelo, D. Luna, R. Luque, J.M. Marinas, A.A. Romero, ChemSusChem 2 (2009) 18-45.

[2] A. Primo, H. García, in: S.L. Suib (Ed.), New and Future Developments in Catalysis, Elsevier, Amsterdam, 2013, pp. 425-449.

[3] H. Ghanbarlou, S. Rowshanzamir, B. Kazeminasab, M.J. Parnian, Journal of Power Sources 273 (2015) 981-989.

[4] Y. Wang, Y. Zhao, W. He, J. Yin, Y. Su, Thin Solid Films 544 (2013) 88-92.

[5] Z. Li, J. Liu, Z. Huang, Y. Yang, C. Xia, F. Li, ACS Catalysis 3 (2013) 839-845.

[6] Y. Roman-Leshkov, C.J. Barrett, Z.Y. Liu, J.A. Dumesic, Nature 447 (2007) 982-985.

[7] A.S. Arico, P. Bruce, B. Scrosati, J.-M. Tarascon, W. van Schalkwijk, Nat Mater 4 (2005) 366-377.

[8] N.J. Divins, I. Angurell, C. Escudero, V. Pérez-Dieste, J. Llorca, Science 346 (2014) 620-623.

[9] C.T. Campbell, Nat Chem 4 (2012) 597-598.

[10] J. Albero, H. Garcia, Journal of Molecular Catalysis A: Chemical 408 (2015) 296-309.

[11] C.N.R. Rao, A.K. Sood, K.S. Subrahmanyam, A. Govindaraj, Angewandte Chemie International Edition 48 (2009) 7752-7777.

[12] S. Navalon, A. Dhakshinamoorthy, M. Alvaro, H. Garcia, Coordination Chemistry Reviews (2016).

[13] E. Yoo, T. Okata, T. Akita, M. Kohyama, J. Nakamura, I. Honma, Nano Letters 9 (2009) 2255-2259.

[14] B. Das, B. Choudhury, A. Gomathi, A.K. Manna, S.K. Pati, C.N.R. Rao, ChemPhysChem 12 (2011) 937-943.

[15] P. Lazar, S. Zhang, K. Šafářová, Q. Li, J.P. Froning, J. Granatier, P. Hobza, R. Zbořil, F. Besenbacher, M. Dong, M. Otyepka, ACS Nano 7 (2013) 1646-1651.

[16] T. Liao, Z. Sun, C. Sun, S.X. Dou, D.J. Searles, Scientific Reports 4 (2014) 6256.

[17] W. Zhang, Y. Li, X. Zeng, S. Peng, Scientific Reports 5 (2015) 10589.

[18] N. Naseri, P. Sangpour, S.H. Mousavi, RSC Advances 4 (2014) 46697-46703.
[19] J. Yu, L. Qi, M. Jaroniec, The Journal of Physical Chemistry C 114 (2010) 13118-13125.
[20] M. Serra, J. Albero, H. García, ChemPhysChem 16 (2015) 1842-1845.
[21] G. Nagasubramanian, A.S. Gioda, A.J. Bard, Journal of The Electrochemical Society 128 (1981) 2158-2164.
[22] M. Hara, T. Kondo, M. Komoda, S. Ikeda, J. N. Kondo, K. Domen, M. Hara, K. Shinohara, A. Tanaka, Chemical Communications (1998) 357-358.
[23] W.-T. Kung, Y.-H. Pai, Y.-K. Hsu, C.-H. Lin, C.-M. Wang, Opt. Express 21 (2013) A221-A228.
[24] Y. Kwon, A. Soon, H. Han, H. Lee, Journal of Materials Chemistry A 3 (2015) 156-162.
[25] D. Zhang, D. Wei, Z. Cui, S. Wang, S. Yang, M. Cao, C. Hu, Physical Chemistry Chemical Physics 16 (2014) 25531-25536.
[26] L.I. Bendavid, E.A. Carter, The Journal of Physical Chemistry B 117 (2013) 15750-15760.
[27] Z. Li, C.V. Ciobanu, J. Hu, J.-P. Palomares-Baez, J.-L. Rodriguez-Lopez, R. Richards, Physical Chemistry Chemical Physics 13 (2011) 2582-2589.
[28] H. Lee, RSC Advances 4 (2014) 41017-41027.
[29] A. Primo, I. Esteve-Adell, J.F. Blandez, A. Dhakshinamoorthy, M. Alvaro, N. Candu, S.M. Coman, V.I. Parvulescu, H. Garcia, Nat Commun 6 (2015).
[30] E. Palomares, M.V. Martinez-Diaz, S.A. Haque, T. Torres, J.R. Durrant, Chemical Communications (2004) 2112-2113.
[31] K. Reimann, K. Syassen, Physical Review B 39 (1989) 11113-11119.
[32] B. Balamurugan, I. Aruna, B.R. Mehta, S.M. Shivaprasad, Physical Review B 69 (2004) 165419.
[33] S. Wu, Z. Yin, Q. He, G. Lu, X. Zhou, H. Zhang, Journal of Materials Chemistry 21 (2011) 3467-3470.
[34] L. Jiang, T. You, P. Yin, Y. Shang, D. Zhang, L. Guo, S. Yang, Nanoscale 5 (2013) 2784-2789.
[35] A. Primo, P. Atienzar, E. Sanchez, J.M. Delgado, H. Garcia, Chemical Communications 48 (2012) 9254-9256.
[36] S. Ikeda, T. Takata, T. Kondo, G. Hitoki, M. Hara, J. N. Kondo, K. Domen, H. Hosono, H. Kawazoe, A. Tanaka, Chemical Communications (1998) 2185-2186.
[37] S. Ikeda, T. Takata, M. Komoda, M. Hara, J. N. Kondo, K. Domen, A. Tanaka, H. Hosono, H. Kawazoe, Physical Chemistry Chemical Physics 1 (1999) 4485-4491.
[38] D.C.B. Alves, R. Silva, D. Voiry, T. Asefa, M. Chhowalla, Materials for Renewable and Sustainable Energy 4 (2015) 1-7.
[39] P. C Ghosh, T. Banerjee, A. Mukherjee, Energy Procedia 54 (2014) 221-227.
[40] S. Kakuta, T. Abe, Electrochemical and Solid-State Letters 12 (2009) P1-P3.
[41] A. Martinez-Garcia, V.K. Vendra, S. Sunkara, P. Haldankar, J. Jasinski, M.K. Sunkara, Journal of Materials Chemistry A 1 (2013) 15235-15241.
[42] D. Mateo, I. Esteve-Adell, J. Albero, J.F.S. Royo, A. Primo, H. Garcia, Nat Commun 7 (2016).
[43] A. Paracchino, V. Laporte, K. Sivula, M. Grätzel, E. Thimsen, Nat Mater 10 (2011) 456-461.